Ionics (2008) 14:183–190
DOI 10.1007/s11581-007-0170-3

ORIGINAL PAPER

Nanostructured transition metal phosphide as negative electrode for lithium-ion batteries

S. Boyanov · K. Annou · C. Villevieille · M. Pelosi · D. Zitoun · L. Monconduit

Received: 7 September 2007 / Accepted: 2 October 2007 / Published online: 9 November 2007

Abstract In the Li-ion technology, the diffusion of Li in the electrode is often limited by the quality of interfaces. Two synthetic approaches are proposed to develop the transition metal phosphides (TMP)/electrolyte interface. The first route consists in the preparation of nickel nanopowder by solution phase synthesis, and the second is based on the electrochemical synthesis of nickel nanorods in a template followed by vaporization of phosphorous. In the former, the nanosized metallic particles are foreseen to be used as starting nanomaterial to directly react with phosphorous agents (P or Li_3P) during the cycling of the lithium battery. A preliminary electrochemical test of the NiP_x nanorods/Li half-cell shows the feasibility of the use of such nanostructured TMP electrode in a Li battery.

Keywords Transition metal phosphide · Nanoparticles · Nanostructuration · Li ion battery

Introduction

Seeking new materials is a challenge that remains the key for the development of energy storage Li-ion systems. Due to its advent on the market, such technology has been using $LiCoO_2$ as positive electrode and a carbonaceous material as negative electrode. For the negative side of the battery, the challenge relies on discovering materials showing greater capacities than graphite while maintaining excellent capacity retention. The transition metal phosphides (TMP) [1] are promising negative electrode materials exhibiting high gravimetric and volumetric capacities associated with low electrode volume expansions. They display different redox reactions depending on the 3d transition metal. With middle and late transition metals (M=Mn, Fe, Co, Ni), it generally proceeds through the conversion of MP_y into a composite electrode made of metallic nanosized particles embedded into a Li_3P matrix ($MP_y + 3yLi \rightarrow yLi_3P + M°$) [2, 3]. These so-called conversion reactions [4] offer a new type of energy storage involving a larger exchange of Li.

In a previous work, we electrochemically tested NiP_2 vs Li [5]. NiP_2 was prepared by high-temperature ceramic route (HT) and by ball milling route (BM). In both cases, the powders are made of shapeless particles having an average size ranging from 5 to 50 μm for the NiP_2-HT sample (Fig. 1a) and from 0.5 to 2 μm for the ball-milled NiP_2-BM sample (Fig. 1b). The voltage composition curves (and in inset, the capacity retention) are shown in Fig. 1b, d. These curves show reversible capacities of 1,000 mAh/g (4,900 mAh/cm^3) and 840 mAh/g (4,100 mAh/cm^3), for NiP_2-HT and -BM, respectively. Both cells show a capacity decay upon cycling that is worse for the Li/NiP_2-BM cell at a C/10 rate and pretty much the same at C/20. The study of the electrochemical mechanism has shown that, during the first discharge, the cubic BM phase undergoes a pure conversion process ($NiP_2 + 6\ Li^+ + 6e^- \rightarrow Ni° + 2Li_3P$) as opposed to a sequential insertion–conversion process for monoclinic HT-NiP_2. Once the first discharge is achieved, both phases were shown to react with Li through a classical conversion process: $NiP_2 + 6Li \leftrightarrow 2Li_3P + Ni°$ [5]. Although the TMP show capacities greater than graphite, as demon-

Paper presented at the 11th EuroConference on the Science and Technology of Ionics, Batz-sur-Mer, Sept. 9–15, 2007.

S. Boyanov · K. Annou · C. Villevieille · M. Pelosi · D. Zitoun · L. Monconduit (✉)
ICG-AIME, CNRS, Université Montpellier 2, Montpellier, France
e-mail: laure.monconduit@univ-montp2.fr

D. Zitoun
e-mail: zitoun@univ-montp2.fr

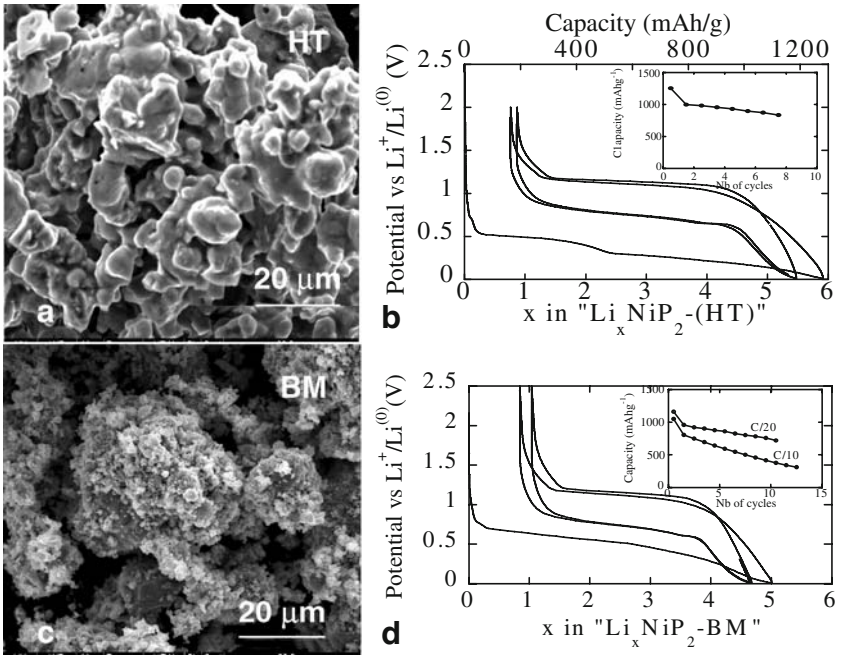

Fig. 1 **a** SEM images of monoclinic NiP_2 prepared by a high temperature ceramic route and **b** by a ball milling route. In **c** the voltage-composition traces for the HT-NiP_2 /Li and **d** for the BM-NiP_2/Li cells cycled at a C/10, rate between 2 to 0 V are shown together with, as *inset*, their capacity retention

strated for NiP_2, their quite low capacity retention still falls short to be suitable for practical applications. The key for exploiting these phosphide-based materials in future applications lies in controlling the kinetics of lithium insertion, thereby lowering the charge/discharge polarization voltage which is currently responsible for the still poor energy performance of negative electrodes based on conversion reactions. To reach this goal, advances in engineering are needed, particularly on TMP. Following this goal, we have succeeded in growing Cu_3P as a thick film over a copper foil by a very simple solid-state reaction at low temperature [6]. More recently, we have explored the growth of NiP_2 onto Ni foam [7]. Using such synthesis route, we could obtain carbon-free self-supported NiP_2 electrodes capable of sustaining high capacities over many cycles with enhanced rate capabilities.

Nanostructuration of electrodes usually aims at enhancing their specific surface area so that the kinetics would be improved, along with a better buffering of the active material volume expansion. This new architecture would lead to a better cycleability. Recently, Simon and coworkers have published a two-step electrode design consisting of the electrochemically assisted templated growth of Cu nanorods onto a current collector followed by electrochemical plating of Fe_3O_4 [8]. Using such electrodes, they demonstrated a great improvement in power density and in capacity retention.

To advance in engineering of the TMP, we propose in this paper to improve the kinetics of reactions of NiP_2 vs Li together with enhancement of their capacity retention by (1) acting at the particle size by the use of novel synthetic routes and (2) designing a new electrode. The first way consists in the preparation of metallic nickel nanopowder by solution phase synthesis. These nickel nanoparticles are foreseen to be embedded in a P or Li_3P matrix before being electrochemically tested vs Li. The second way is based on the electrochemical template synthesis of nickel nanorods. The as-obtained metallic pillars are then thermally treated under phosphorous vapor leading NiP_2 nanorods.

Experimental details

Synthesis

Nanoparticles by solution phase synthesis

Hexagonal close-packed nickel has been synthesized through reduction of nickel diacetylacetonate $Ni(acac)_2$ at 180–300 °C. All reactions were carried out in an argon atmosphere on a vacuum line. Anhydrous $Ni(acac)_2$ (Merck, 98%), benzyl alcohol (BA; Acros, 99+%), benzylamine (Acros 99.5+%), 1-hexadecylamine straight-chained (Acros 90%), and oleylamine (Acros 70%) were used without further purification after a degassing procedure. Synthesis was carried out in refluxing solvent (benzylamine, benzyl alcohol, oleylamine, hexadecylamine, octadecene/hexadecylamine). In a typical synthesis, the nickel nanoparticles

were prepared by reacting anhydrous $Ni(acac)_2$ in boiling benzyl alcohol ($[Ni^{2+}]$=0.2 M) in a three-neck balloon under an argon atmosphere. Upon heating, the color of the solution changed from green to black, indicating that colloidal nanoparticles were generated. The black solution was aged at 180 °C for 2 h and cooled down to room temperature. The nanoparticles were redispersed by adding an excess of heptane. Before any treatment, the solution was kept in an ultrasound bath for 10 min. The black powder was retrieved by centrifugation, and the procedure was repeated at least three times to wash all organic reagents and by-products. Following this synthetic route, the overall yield synthesis was at least 65% based on the amount of Ni measured with energy-dispersive X-ray spectroscopy (EDX).

In another synthetic pathway, the syntheses could be carried out in an autoclave at higher temperature (up to 250 °C). The synthesis was then continued for 48 h to complete the reaction, the post-synthesis procedure being the same as previously mentioned.

The proposed reactional mechanism is:

$$R-NH_2 \rightarrow R=NH+{}^1/_2\,H_{2(g)}$$
$$Ni^{2+}+H_{2(g)} \rightarrow Ni^{(0)}+2H^+ \quad \text{(reduction step)}$$
$$R-NH_2+H^+ \rightarrow R-NH_3^+$$

Following the same solution phase synthesis, different solvents were tested. In the case of hexadecylamine, the amine to nickel stoichiometry was fixed to two equivalents.

Nanowires by electrosynthesis

Ni nanorods are grown by direct electrodeposition of nickel through the pores of an anodized alumina oxide membrane which has been set on top of a copper or nickel foil. Anodic aluminum oxide (AAO) Anodisc® 13 (0.02 μm, 13 mm) were purchased from Whatman®. The electrolyte solution was prepared using a standard procedure $NiSO_4$, $6H_2O$ (40 g/200 ml), H_3BO_3 (5 g/200 ml), $NiCl_2$, $6H_2O$ (1 g/200 ml). The AAO template is deposited on a metallic Cu or Ni sheet (≈1 cm^2). The metallic surface was thoroughly washed to ensure good contact with the membrane. The membrane was already impregnated for 24 h in the electrolyte solution. The standard Ni deposition was carried out with a stable potential of 1.5 V and a current between 10 and 30 mA. The deposition was continued for 30 to 90 min depending on the length of wires desired (15–45 μm). A schematic description of the process is shown in Fig. 2.

After deposition, the film was washed with distilled water. Then, alumina (Al_2O_3) was dissolved in an aqueous 5 M sodium hydroxide solution. Finally, the film was washed with water and acidic nickel solution to remove any oxide traces on the surface.

Structural studies of the as-obtained Ni powders or nanowires were done by X-ray diffraction and transmission electron microscopy (TEM).

P-vaporization on Ni nanorods

Ni nanorods are disposed in one compartment of a two-compartment evacuated and sealed quartz ampoule with, in the other compartment, stoichiometric amounts of red phosphorous powders. A survey of various temperatures (ranging from 350 to 400 °C) and reaction times (2 to 14 h) was conducted.

The quartz vessels were placed into an oven. Once the selected annealing temperature profile was completed, the oven was turned off, the tube opened, and the "phosphorized" Ni recovered substrate was characterized by X-ray analysis and by both scanning electron microscopy (SEM) and EDX.

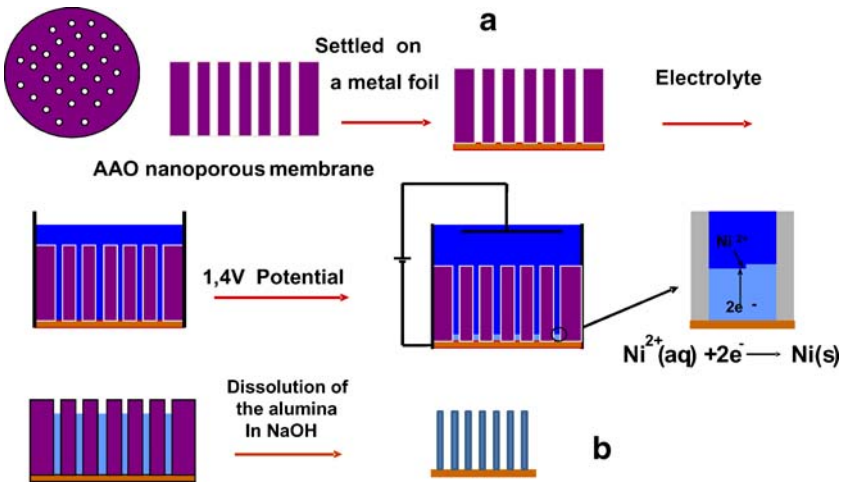

Fig. 2 **a** A schematic description of the electrochemical cell used for the template synthesis of the nanostructured Ni current collector. **b** Schematic description of the nanostructured current collector at the end of the electrolysis before and after dissolution of the AAO membrane

X ray diffraction

X-ray diffraction (XRD) measurements on the powdered Ni samples or on the phosphorized Ni nanowires were performed on a Philips X-pert diffractometer using the CuK_α radiation.

Microscopies

The powder morphology of pristine materials was determined by SEM and TEM. Quantitative EDX analysis of the nanopowders and nanowires shows the molar ratio content of the main elemental components.

Electrochemical tests

Swagelok-type cells were assembled in an argon-filled glove box and cycled using a Mac Pile automatic cycling/data recording systems (Biologic, Claix, France) in a potential window between 2.5 V (or 2 V) and 0.02 V vs Li^+/Li^0 and a cycling rate of *C*/*n* (that is one lithium per formula unit in *n* hours). These cells comprise a Li metal disc as the negative electrode, a Whatman GF/D borosilicate glass fiber sheet saturated with a 1 M $LiPF_6$ in ethylene carbonate, dimethyl carbonate (1:1 in weight) as the electrolyte, and a nanostructured NiP_2 on Cu foil as positive electrode.

Results

Nanoparticles by solution phase synthesis

We performed a solution phase synthesis towards Ni nanoparticles in various conditions of temperature (180–300 °C). The reaction yields an amount of pure inorganic material with clean and accessible surface. The chemical reduction involves the reduction of Ni(II) acetylacetonate to Ni(0) in an organic solvent (amine, alcohol), which also acts as a reducing and stabilizing agent.

Table 1 summarizes the reaction conditions of the solution nickel reduction and the corresponding EDX analysis. From EDX analysis, a massic yield is calculated.

Carbon was also found in the EDX analysis, which comes from surface contamination mainly due to the adsorption of ligand and by-product that were not completely removed by the surface-cleaning step. Table 1

Table 1 Solution phase synthesis conditions and EDX results

Solvent	Type of synthesis	Thermal treatment	Samples	SEM/ TEMimage	XRD results	EDX composition (%)
Benzylamine	Balloon	180 °C/2 h	Yield 34% black magnetic powder	–	hcp	C, 34.5 O, 17.7 Ni, 47.8
	Autoclave	250 °C/48 h	Yield 86% magnetic black powder	–	hcp+ ε fcc	C, 11.5 O, 2.5 Ni, 86.0
Benzylalcohol	Balloon	180 °C/2 h	Yield 64% gray magnetic powder	Fig. 4a,b	fcc Fig. 3a	C, 15.9 O, 6.3 Ni, 77. 8
	Autoclave	250 °C/48 h	Yield 66% black-gray magnetic powder	–	hcp+fcc	C, 26.6 O, 3.4 Ni, 70.0
Oleylamine	Balloon	110 °C/0.5 h 220 °C/2 h	Low yield <10%	–	hcp	C, 69.80 O, 9.21 Ni, 20.99
		300 °C/2 h	Low yield 18% black magnetic powder		hcp	C, 51.0 O, 5.8 Ni, 43.2
Octadecene + Hexadecylamine	Balloon	230 °C/2 h	Yield 62% black powder	Fig. 4c,d	hcp Fig. 3b	C, 50.4 O, 3.0 Ni, 46.6
	Autoclave	250 °C/48 h	Yield 54% gray magnetic powder	–	hcp	C, 54.8 O, 11.2 Ni, 34.0
Hexadecylamine	Autoclave	250 °C 48 h	Yield 14% black magnetic powder	–	hcp + ε fcc	C, 78.0 O, 2.0 Ni, 18.0

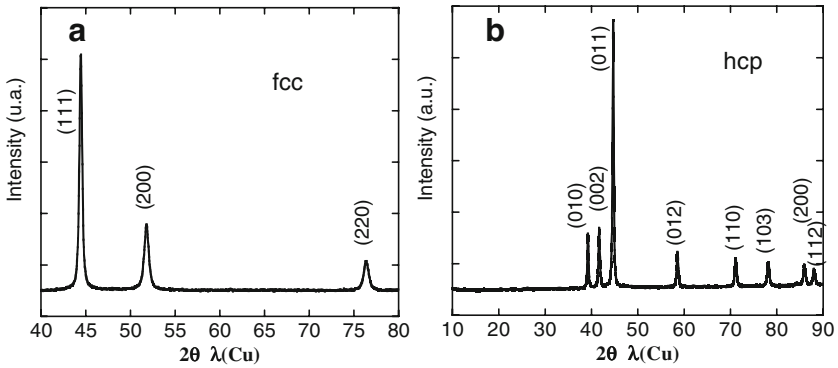

Fig. 3 XRD pattern of Ni nanoparticles prepared **a** in benzyl alcohol in balloon and **b** in octadecene–hexadecylamine (balloon 180 °C)

clearly indicates that the solvent strongly influences the yield and the purity of the product. Benzyl alcohol and benzyl amine are well known in non-hydrolytic sol–gel chemistry to be easily washed out from the inorganic surface. On the contrary, long-chain amine (such as oleylamine or hexadecylamine) would be coordinated to the surface atom, which explains the higher carbon ratio in these samples. For each route, the best reaction yields are obtained with the benzyl alcohol in balloon or in autoclave, 78 and 70%, respectively, and with the solvents octadecene/hexadecylamine in balloon (47%). These two syntheses will be investigated in detail below and will be referred to as the BA or hexadecylamine (HDA) route.

Structural characterization by XRD and SEM

Figure 3a shows the X-ray diffraction powder pattern collected from the BA and HAD samples. The pattern for BA sample shows three broad peaks corresponding to fcc Ni (1 1 1), (2 0 0), and (2 2 0), while for the HAD sample (see Fig. 3) all the peaks are indexed as hcp Ni (0 1 0), (0 0 2), (0 1 1), (0 1 2), (1 1 0), (1 0 3), (1 1 2), and (2 0 1) [9]. No other peaks that belong to impurities could be detected in these XRD patterns. Hcp nickel was the main phase that could be deduced from XRD for all other syntheses performed. Interestingly, a slight increase of reaction temperature for the benzyl alcohol route leads to hcp nickel. Other amines such as benzylamine and oleylamine at various temperatures were used in the reduction process, and the corresponding XRD patterns display only hcp Ni. The stabilization of the high-temperature phase (namely hcp) is a very common phenomenon for nanocrystalline materials [10]. The surface energy strongly modifies the stability of each phase. It was suggested that the solvents influence the growth structure and morphology of the crystals because the solvents could selectively control the surface energy of

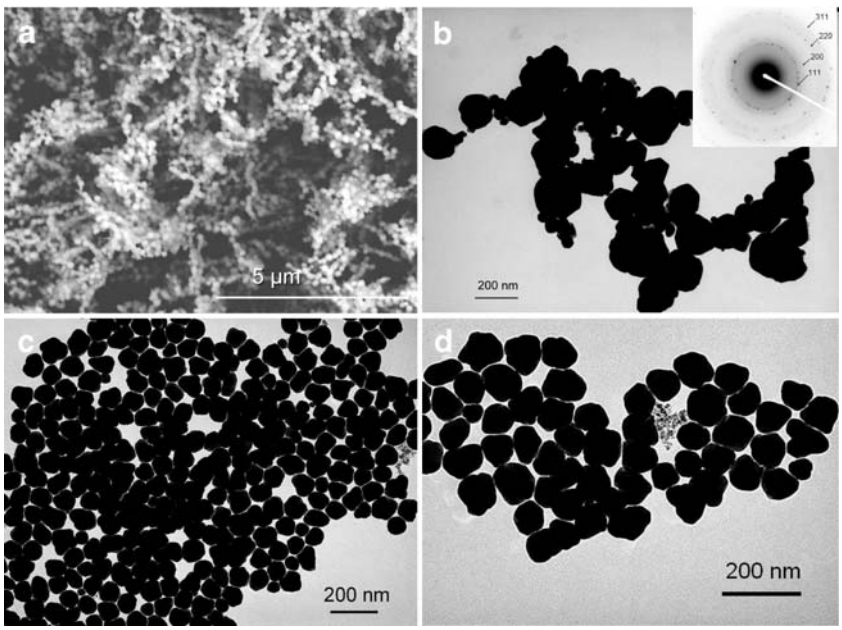

Fig. 4 **a** SEM and **b** TEM images of Ni nanoparticles prepared in benzyl alcohol in balloon (180 °C/2 h) and **c**, **d** TEM images of Ni nanoparticles prepared in octadecene–hexadecylamine (balloon 230 °C/2 h)

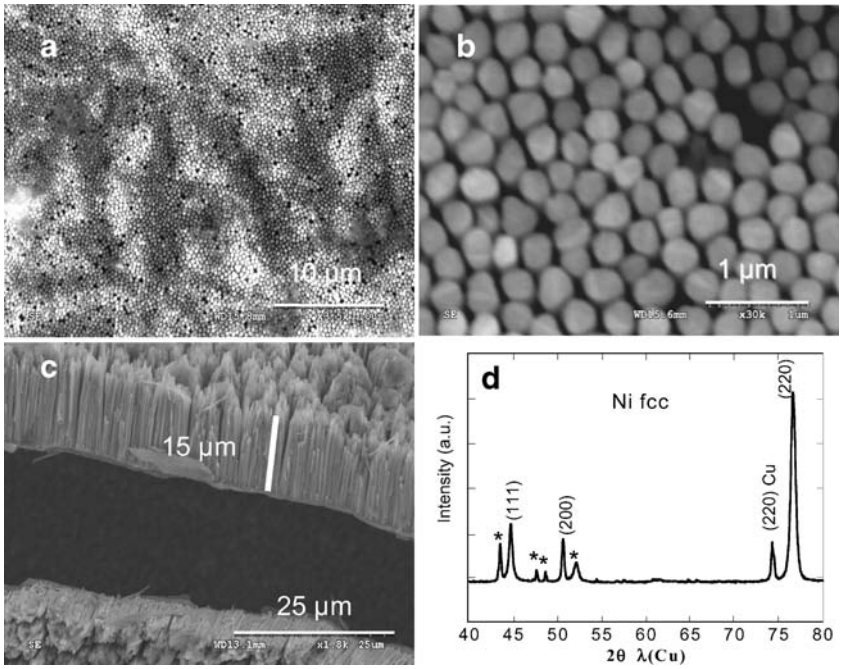

Fig. 5 SEM images. Top view of the Ni nanorods obtained after electrolysis and membrane removal. **a** ×3,500 magnification and **b** ×30k magnification. **c** Cross-sectional view of Ni pillars and **d** corresponding XRD pattern (holder peaks are identified by *stars*)

different crystallographic faces [11, 12]. Another key parameter lies in the kinetics of the reaction; in the present case, the driving force towards the synthesis of hcp nickel is the nucleation rate of hcp nanocrystals seeds. Indeed, hcp nickel is obtained with higher temperature (from 180 to 250 °C) or reducing power (from alcohol to amine).

To further reveal the morphology and structure of Ni nanoparticles, TEM and SEM were carried out for all the samples.

The samples BA and HDA on Fig. 4a–d, respectively, consist of a large quantity of nearly spherical isolated nanoparticles. The average particle size reaches the value of D=90±30 nm. Electron diffraction pattern (Fig. 4b, inset) confirms the fcc phase deduced from XRD analysis for the BA sample.

Nanowires by electrochemically templated synthesis

As schematically described in Fig. 2, an electrochemical method involving reduction of Ni^{2+} ions to Ni (0) in a Swagelok® cell was employed to yield nickel nanowires on a Ni or Cu substrate. AAO was used as a template to direct the nanowire growth.

Figure 5a–c shows top and cross-section views, respectively, of the Ni nanopillar current collectors in AAO after membrane removal. The Cu foil is covered with uniformly distributed nickel rods with diameters of 250–400 nm, defined by the pore size of the alumina membrane and a height of 10–15 µm. The associated XRD pattern on Fig. 5c shows three broad peaks corresponding to fcc Ni (1 1 1), (2 0 0), and (2 2 0).

Phosphorous vaporization

Table 2 summarizes the thermal conditions used for the phosphorous vaporization on the Ni nanopillars.

Before evaluating the reaction of the phosphorous vapor on the Ni nanorods, we checked the effect of a 350 °C heat treatment. Figure 6b shows that the nanostructure of the Ni pillars is kept under 350 °C despite a small aggregation at the top of the nanopillars.

The different temperature treatments with P showed that the nanostructure was fully consumed for the temperatures higher than 400 °C. In contrast, we experienced that in lowering the temperature below 350 °C, one could not obtain the NiP_x phase independently of the reacting time.

Table 2 Thermal treatments conditions of the P vaporization and resulting Ni/P ratio deduced from the EDX analysis

Temperature (°C)	Number of hours	Membrane/ substrate	Atomic % Ni/P (EDX)	Observations
350	2	Without/Cu	85/15	Nanostructured
350	4	Without/Cu	86/14	Nanostructured
350	6	Without/Cu	91/9	Nanostructured
350	4	With/Cu	94/6	Nanostructured
350	14	Without/Cu	70/30	Nanostructured
350	14	Without/Ni	50/50	Destroyed
350	14	With/Cu	40/60	Nanostructured
400	4	Without/Cu	55/45	Nanostructured
400	4	Without/Ni	45/55	Destroyed

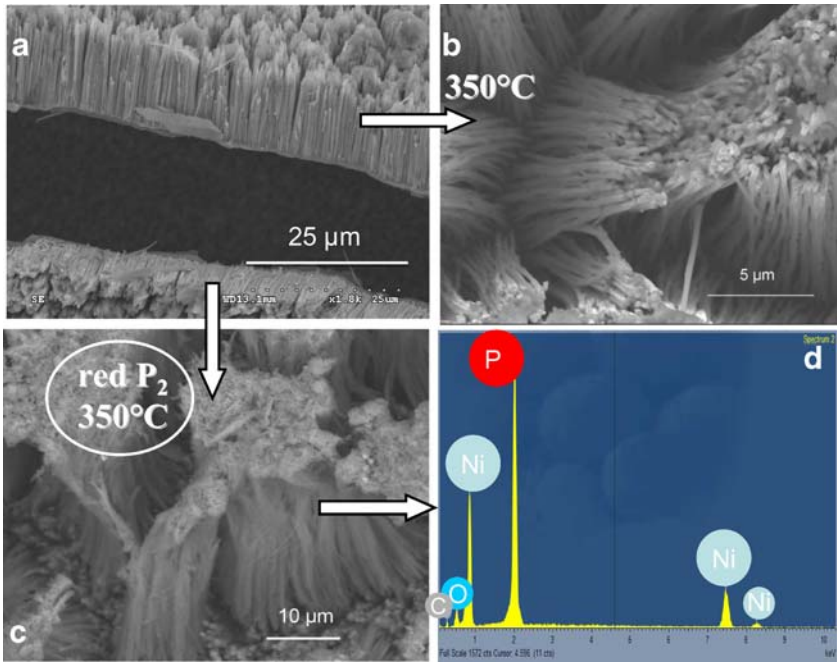

Fig. 6 TEM images. Cross-sectional view of Ni nanopillars **a** pristine, **b** after 350 °C heat treatment, and **c** after phosphorous 350 °C/14 h heat treatment

Thus, we fixed the annealing temperature at 350 °C and varied the reacting time from 2 to 14 h. As shown in Fig. 6c, for a Ni sample (on Cu substrate) treated 14 h at 350 °C, the nanostructure seems to be preserved. The associated EDX analysis reports the 40:60 atomic Ni/P ratio, indicating that NiP_2 is probably formed. The low excess of Ni could be due to a partial reaction of the Ni with phosphorous, principally at the core of the nanopillars. Surprisingly, the Ni pillars on Ni substrate are fully destroyed during the phosphorous vaporization.

A preliminary electrochemical test vs lithium

A first electrochemical test of the as-phosphorized Ni pillars (350 °C/14 h) in a Li half-cell is presented in Fig. 7. The shape of the galvanostatic discharge and charge curves, as well as the associated potential, appears to be very similar to those obtained from the NiP_2-BM sample (Fig. 1c). The amount of NiP_2 nanorods formed on the copper foil is tricky to evaluate and, therefore, the lithium insertion/extraction and the specific capacity are also difficult to calculate (the *x* scale on the galvanostatic curve is arbitrary). However, this first electrochemical signature shows that the lithium insertion (Fig. 7a) and extraction (Fig. 7b) are very reproducible on the first two cycles. However, the lithium insertion upon discharge is larger than the lithium extraction on the following charge. This preliminary electrochemical study of the nanopillars shows that nanostructured TMP can be effective as a negative electrode in lithium-ion battery.

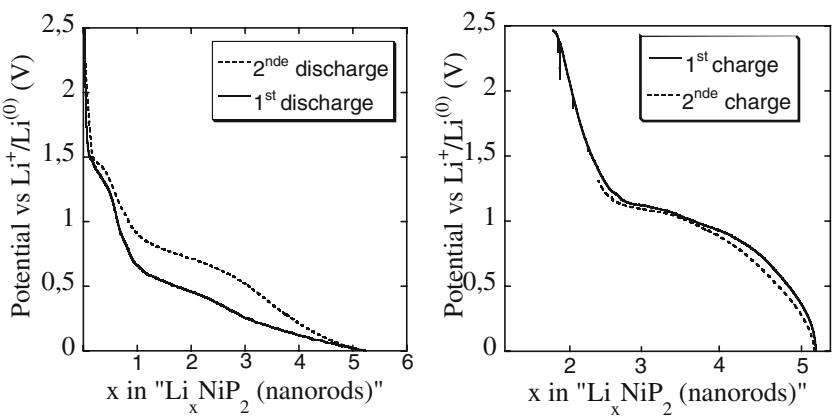

Fig. 7 Voltage–composition curve for a Li half-cell using a nanorod NiP_x sample as the positive electrodes and cycled between 2.5 and 0 V

Conclusion

The use of nanomaterials is known to improve the rate capabilities of solid-state electrodes used in lithium batteries because of the small diffusion lengths. Following this goal, we developed new synthetic approaches that yield nanocrystalline transition metal phosphides with a fine tuning of composition, morphology, and structure.

We succeeded in the preparation of Ni nanoparticles with diameters less than 100 nm. The different analyses carried out showed that the obtained nickel powder consists of nanosized Ni particles with a limited oxidized fraction with regards to its high surface area. This synthesis presents the great advantage of an accessible surface for further electrochemical studies. In the near future, several routes will be used to embed the as-prepared metallic nanoparticles in a phosphorous matrix, either red P or Li_3P. The Ni/2P composite electrode will be tested vs Li in discharge, while the $Ni/2Li_3P$ mixture will be tested vs Li upon charge. From these experiences, the electrochemical mechanism and the associated performances will be compared with the ones measured from BM and HT-NiP_2. This exploratory work is expected (1) to highlight the conversion mechanism of NiP_2/Li especially upon charge and (2) to better identify the surface electrolyte interface (SEI) occurring at low potential and the associated limitations.

The second approach consisted in growing nanostructured NiP_x electrode through a vapor phase transport process on Ni nanorods. These nickel phosphides self-supported electrodes are expected to produce efficient negative electrodes, thanks to the rate capability and the retention efficiency of the resulting battery (two of the well-known limitations of the lithium-ion technology). The first electrochemical test presented in this paper is promising. These new self-supported electrodes, based on chemically made interfaces, offer new opportunities to fully exploit the capacity gains provided by phosphide materials. Needless to say, further optimization work remains to be done to use phosphides in the Li-ion cells.

References

1. Doublet ML, Lemoigno F, Gillot F, Monconduit L (2002) Chem Mat 14(10):4126
2. Gillot F, Monconduit L, Morcrette M, Doublet M-L, Dupont L, Tarascon J-M (2005) Chem Mat 17(14):3627
3. Boyanov S, Bernardi J, Gillot F, Dupont L, Womes M, Tarascon J-M, Monconduit L, Doublet ML (2006) Chem Mat 18:3531
4. Poizot P, Laruelle S, Grugeon S, Dupont L, Tarascon J-M (2000) Nature 407:496–499
5. Gillot F, Boyanov S, Dupont L, Doublet M-L, Morcrette M, Monconduit L, Tarascon J-M (2005) Chem Mat 17(25):6327–6337
6. Pfeiffer H, Tancret F, Bichat MP, Monconduit L, Favier F, Brousse T (2004) Electrochem Commun 6:263–267
7. Gillot F, Tarascon J-M, Monconduit L (2006) PCT Int Appl 34pp. CODEN: PIXXD2 WO 2006123050 A1 20061123
8. Taberna P-L, Mitra S, Poizot P, Simon P, Tarascon J-M (2006) Nature Materials 5:567
9. Carturan G, Cocco G, Enzo S, Ganzerla R, Lenarda M (1988) Mater Lett 7:47
10. Jeon YT, Moon JY, Lee GH, Park J, Chang YM (2006) J Phys Chem B 110:1187–1191
11. Lee SM, Cho SN, Cheon J (2003) Adv Mater 15:441
12. Dinega DP, Bawendi MG (1999) Angew Chem Int Ed Engl 38:1788